


Article

Deriving Spatio-Temporal Development of Ground Subsidence Due to Subway Construction and Operation in Delta Regions with PS-InSAR Data: A Case Study in Guangzhou, China

Huiqiang Wang¹, Guangcai Feng^{1,*}, Bing Xu^{1,*}, Yongping Yu², Zhiwei Li¹ , Yanan Du¹ and Jianjun Zhu¹

¹ School of Geosciences and Info-Physics, Central South University, Changsha 410083, China; wanghuiqiang@csu.edu.cn (H.W.); zwli@csu.edu.cn (Z.L.); yndu_csu@csu.edu.cn (Y.D.); zjj@csu.edu.cn (J.Z.)

² Guangzhou Urban Planning & Design Survey Research Institute, Guangzhou, 510060, China; yongpingyu@yahoo.com

* Correspondence: fredgps@csu.edu.cn (G.F.); xubing@csu.edu.cn (B.X.); Tel.: +86-0731-888-30573 (G.F.)

Received: 17 July 2017; Accepted: 23 September 2017; Published: 28 September 2017

Abstract: Subways have been an important method for relieving traffic pressures in urban areas, but ground subsidence, during construction and operation, can be a serious problem as it may affect the safety of its operation and that of the surrounding buildings. Thus, conducting long-term ground deformation monitoring and modeling for subway networks are essential. Compared with traditional geodetic methods, the Persistent Scatterer Interferometric Synthetic Aperture Radar (PS-InSAR) technique offers wider coverage and denser measurements along subway lines. In this study, we mapped the surface deformation of the Guangzhou subway network with Advanced Synthetic Aperture Radar (ASAR) and Phased Array Type L-band Synthetic Aperture Radar (PALSAR) data using the Interferometric Point Target Analysis (IPTA) technique. The results indicate that newly excavated tunnels have regional subsidence with an average rate of more than 8 mm/year, as found on Lines Two, Three, Six, and GuangFo (GF). Furthermore, we determined the spatio-temporal subsidence behavior of subways with PALSAR in delta areas using Peck's formula and the logistic time model. We estimated the tunneling-related parameters in soft soil areas, which had not been previously explored. We examined a section of line GF, as an example, to estimate the ground settlement trough development. The results showed the maximum settlement increased from −5.2 mm to −23.6 mm and its ground loss ratio ranged from 1.5–8.7% between 13 July 2008 and 19 January 2011. In addition, we found that the tunnels in line GF will become stable after a period of about 2300 days in peak subsidence areas. The results show that the proposed approach can help explain the dynamic ground subsidence along a metro line. This study can provide references for urban subway projects in delta areas, and for the risk assessment of nearby buildings and underground pipelines along metro lines.

Keywords: Guangzhou subway network; IPTA; ground settlement trough; Peck's formula; logistic time model

1. Introduction

The excellent climate, beautiful landscape, and convenient waterway communication have contributed to the favorable economic development of delta regions around the world, such as Guangzhou, Shanghai, Shenzhen, and Beijing in China, Mexico City in Mexico, and Bangkok in Thailand. Along with rapid city development, the population in these regions has been growing exponentially. Around the world, more than 600 million people live in cities on or near river

deltas, which has increased the demand for rapid transportation. Many cities have made enormous efforts to expand their underground subway networks. However, vulnerable geological conditions plus sediment loading, compaction, and human activities, including groundwater and hydrocarbon extraction, have led to different degrees of subsidence. These human activities all significantly impact subway construction and operation, so surface subsidence monitoring along any subway under construction and operation is necessary.

Geodetic methods, such as levelling and topographic measurements, are currently good solutions for monitoring the displacements induced by tunneling. However, the effectiveness of these techniques strongly depends on their spatial density [1–3] because sparse geodetic observations cannot provide a full picture of the sinking process along metro lines or detect ground deformation variation in both time and space [4]. Thus, understanding and accurately estimating the tunneling-related parameters using those datasets are difficult. Interferometric Synthetic Aperture Radar (InSAR) [5–7], a satellite-based technique, offers high precision (the millimeter level), high spatial resolution and wide coverage measurements for surface deformations [8–15]. Because of this, InSAR is well suited for monitoring the surface deformation of subway lines. However, only a few ground deformations, related to subways in delta areas, have been identified [16–22], and little work has used InSAR observation to study tunneling parameters, such as the maximum settlement, ground loss, and settlement trough width. This study attempted to use InSAR measurements to monitor the surface deformation along subway lines and determine the tunneling-induced deformation parameters.

In this study, Guangzhou city in China was selected as the study area. We monitored the deformation of the Guangzhou subway network from 2007 to 2011 with 29 ENVISAT and Advanced Synthetic Aperture Radar (ASAR) images and 20 Advanced Land Observation Satellite (ALOS) and Phased Array Type L-band Synthetic Aperture Radar (PALSAR) images using the Interferometric Point Target Analysis (IPTA) technique. Based on the obtained ground subsidence data, we used Peck's formula [23,24] and the logistic time model [25–28] to reveal the tunneling parameters and long-term subsidence behavior of subway tunnels. Finally, some implications are provided in the discussion section.

2. Study Area, InSAR Dataset, and Methods

2.1. Study Area

Guangzhou, located on the Pearl River delta, is the third largest city in China. The local population is 13 million, and the floating population is around 20 million [29,30]. At the end of 2013, the city had nine subway lines, lines one, two, three, four, five, six, eight, Zhujiang New Town automated people mover system (APM), and GuangFo (GF), and 170 stations with a total mileage of about 270 km in operation (Figure 1) [31]. Details of these metro lines are listed in Table A1. The Guangzhou subway network is still under expansion, and will have 35 subway lines, with a total mileage of about 981 km by the end of 2025 [31]. However, frequent subsidence and geohazards close to the subway network have caused concerns about the safety and possible risks involved in the operation of the subway. Subsidence can be caused by fragile hydrogeological conditions, such as alluvial clay and hidden karst, together with improper tunneling construction and vibration during subway operation. So, it is a unique area to monitor subway deformation and the change in tunneling-induced parameters. A stack of 29 ENVISAT and 20 ALOS images, acquired from an ascending orbit from April 2007 to January 2011, were used to map the surface deformation with GAMMA software. The InSAR data provided ground deformation monitoring results for the whole Guangzhou subway network (Figure 1). Details of the Synthetic Aperture Radar (SAR) data information are listed in Table A2.

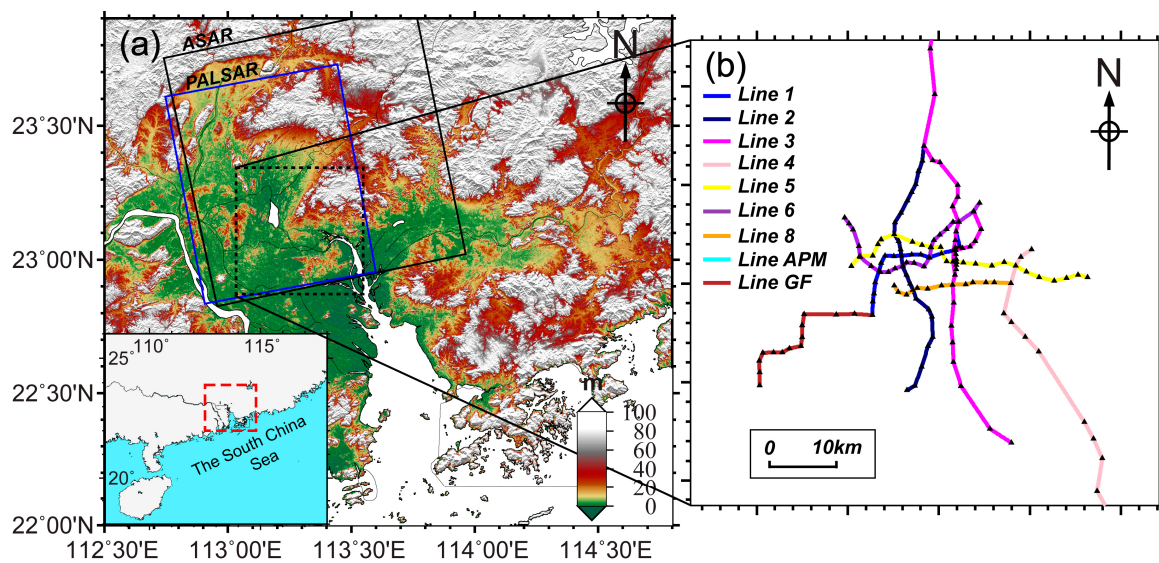


Figure 1. Study area and Synthetic Aperture Radar (SAR) data coverage. (a) Background setting (inset) of the research domain and the SAR data coverage. Black and blue rectangles represent the Advanced Synthetic Aperture Radar (ASAR) and Phased Array Type L-band Synthetic Aperture Radar (PALSAR) coverage, respectively; (b) Metro line distribution map of Guangzhou, including lines one, two, three, four, five, six, eight, APM, and GuangFo (GF). Black triangles are the subway station locations.

2.2. InSAR Data Processing

We selected Interferometric Point Target Analysis (IPTA) [32,33] to monitor the ground subsidence of the Guangzhou region. We chose the ASAR image from 29 September 2008 and the PALSAR image from 16 January 2010 as master images to minimize the effects of normal and temporal baselines during processing. All interferograms were generated corresponding to the master images. These SAR data were processed by conventional IPTA procedures. Topographic phase contributions were removed from each point target (PT) by the 30 m Shuttle Radar Topography Mission (SRTM) Digital Elevation Model (DEM). Satellite orbital errors often cause phase errors, thereby producing low-frequency fringes [34–37]. We re-estimated the baseline parameters from the unwrapped point phase and the DEM heights. The IPTA results included the height estimate, the average displacement rate, and the uncertainties of the height estimate and displacement rate. Then, the time series of the surface displacement were computed based on the reference images, which were the ASAR image from 23 April 2007 and the PALSAR image from 11 July 2007.

Figure 2a,b show the average displacement rates of Guangzhou and Foshan areas from 2007 to 2011, obtained by ASAR and PALSAR images. The rate uncertainties are shown in Figure A1. Their results exhibit good consistency in both deformation magnitude and extent, though they have different wavelengths. The most remarkable subsidence occurred in Foshan with an average rate of over 15 mm/year (left bottom of Figure 2a,b marked by a red dashed line). Other subsidence was limited in size and scattered across the city, with the subsidence rates ranging from 5 to 15 mm/year.

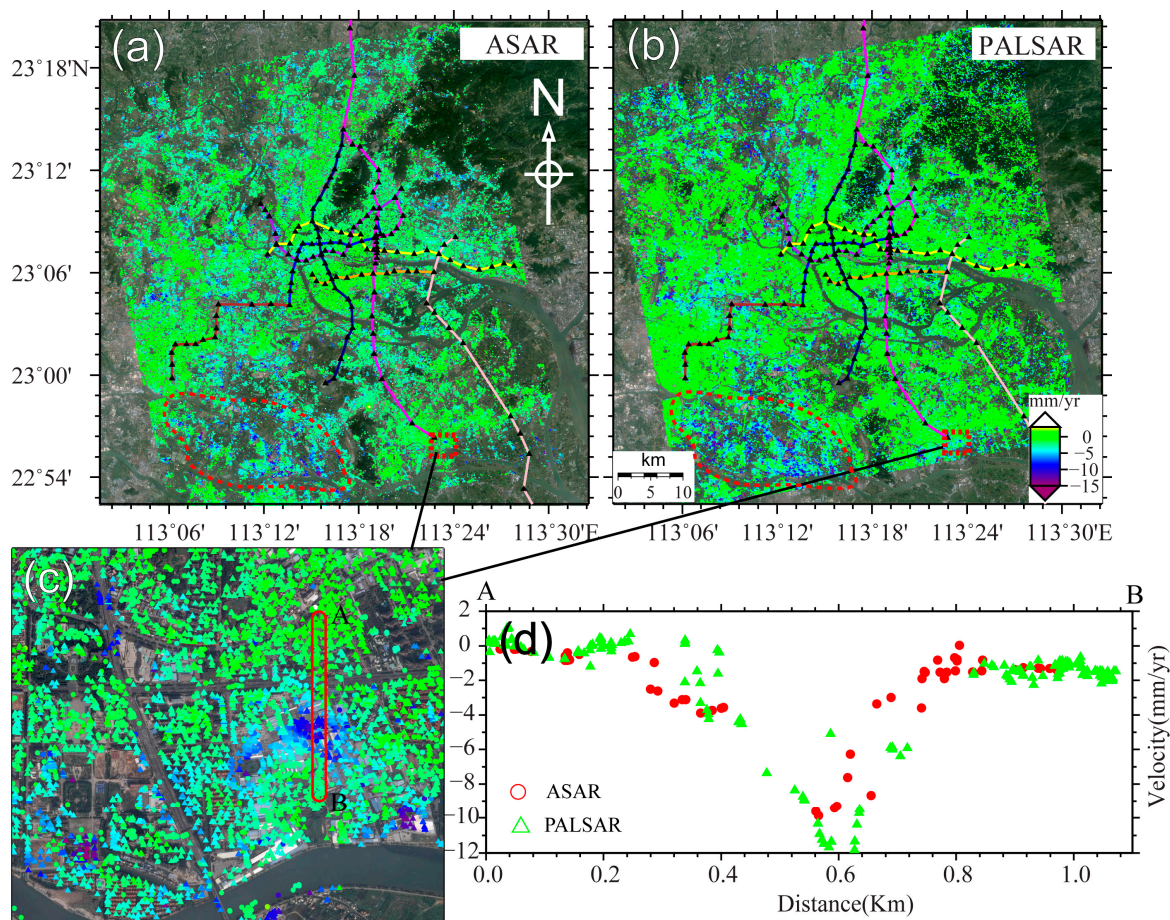


Figure 2. Deformation rates generated by ASAR and PALSAR datasets for the whole study area and their cross validation: (a) the deformation velocity ASAR map; (b) the deformation velocity PALSAR map; (c) the validation area; and (d) the profile map of AB in (c).

2.3. Calibration and Validation

SAR-based results are differential measurements, meaning the PT displacements are relative to a reference point. We used the leveling results to calibrate the SAR results and obtain “absolute” displacements. Our results show that most ground displacement rates are <20 mm/year and the vertical subsidence is the main deformation component. From the InSAR observations, vertical subsidence was usually accompanied by horizontal deformation. However, in this study, we only focused on the spatio-temporal development of vertical subsidence. So, we used a simulation experiment to evaluate the effect of horizontal and vertical displacement on the line of sight (LOS) displacement, and found that the non-horizontal assumption for calculating vertical deformation, in this case, was reasonable (Appendix B). Thus, we assumed that the horizontal ground displacement was negligible and transformed the IPTA results from LOS to the vertical direction, then compared it with the leveling results. In order to accurately evaluate the reliability of the IPTA results, we divided the 63 leveling points in Figure 3a into two parts, i.e., 49 stable points with a mean absolute rate of <1 mm/year, and 14 subsiding points with a mean absolute rate of >1 mm/year). Finally, we calculated the mean and the standard deviation of the difference between the IPTA results and leveling results (Figure 3b,c). The results show that the mean of the differences is less than 0.7 mm/year and the standard deviations range from 0.5 to 1.6 mm/year. This confirms the accuracy and reliability of our results.

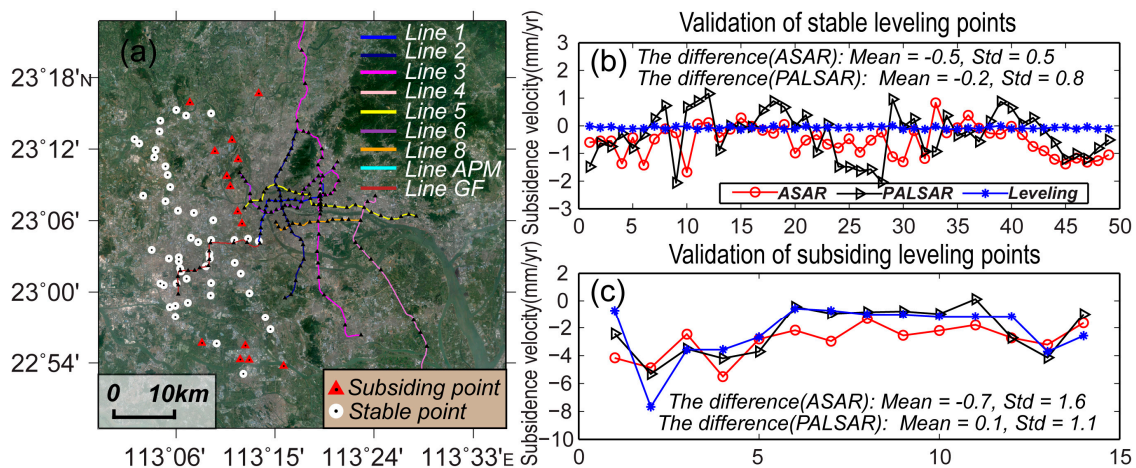


Figure 3. (a) Distribution of leveling points and location of Guangzhou subway network and (b,c) validations of IPTA results with leveling points.

The accuracy and reliability of the IPTA results are dependent on the available dataset (number of scenes, sampling, and duration), deformation features (scale and speed of the ground movements), and surface features (PT density). In this study, the accuracy of the IPTA subsidence rate was in the order of 0.5 mm/year and 1 mm/year for the ASAR and PALSAR results (Figure A1). We randomly selected a subsidence funnel area (Figure 2c) to illustrate the profile across the funnel (profile AB). The magnitude and extent of the deformation are similar to that shown in Figure 2d. Both mutual and external comparisons showed the two results are reliable.

3. Ground Subsidence of the Guangzhou Subway Network

In this study, the ground subsidence of the whole Guangzhou city was detected with both ASAR and PALSAR data as outlined in Section 2. As Figure 2 shows, small scale subsidence is scattered across the city. The scattered subsidence was caused by tunnel excavation during subway construction, with slow soil consolidation around the tunnel, and the cyclic loading of trains [16,18]. Compared with the ASAR data results (Figure 2), the PALSAR results had higher PT density and coherence, benefiting from the better penetration of the L-band satellite. So, we selected the PALSAR results to analyze the subsidence along each metro line.

3.1. Line Two

As Figure 4a shows, the middle part of Line Two is stable, and most subsiding areas are distributed around the north and south ends, indicated by the white dashed boxes. This is because the middle section, between the Sanyuanli station and Jiangnanxi station, was completed at the end of 2002, and was expanded southward and northward after 2007 (Table A1). Furthermore, these subsiding areas in Figure 4b,c are surrounding stations, such as Baiyun Culture Square and Dongxiaonan stations. The peak subsiding areas (>15 mm/year) in Figure 4d are in the section between Huijiang and Nanpu stations. This may be related to the local geological conditions, which will be discussed in Section 5.2.

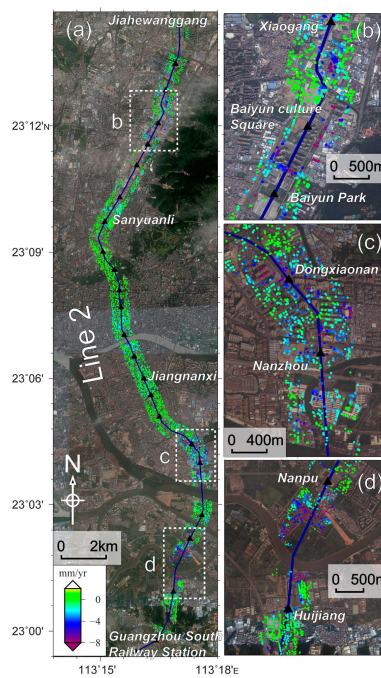


Figure 4. (a) PALSAR deformation rate map of Line Two. Regions b, c, and d, marked by white dashed rectangles, are the three subsiding areas along Line Two, and their enlarged figures are shown in (b), (c), and (d), respectively.

3.2. Line Three

The south part of Line Three (Figure 5d) started operating at the end of 2006, and was expanded northward three years later (Figure 5a), so the south part is more stable. In the north part, there are two obvious subsiding areas near the Longgui and Tonghe stations, represented by the white dashed boxes in Figure 5a. The highest displacement exceeded 8 mm/year (Figure 5b,c). There are two small-scale subsiding areas in the south section, indicated by the white dashed boxes in Figure 5e,f, at approximately 7 mm/year. One is adjacent to the Xiajiao station and the other is around the Shiqiao station. The most severe deformation occurred in areas with buildings or road intersections, which may be caused by the combined action of subway construction and other factors, like underground water extraction, but this needs to be verified with field work.

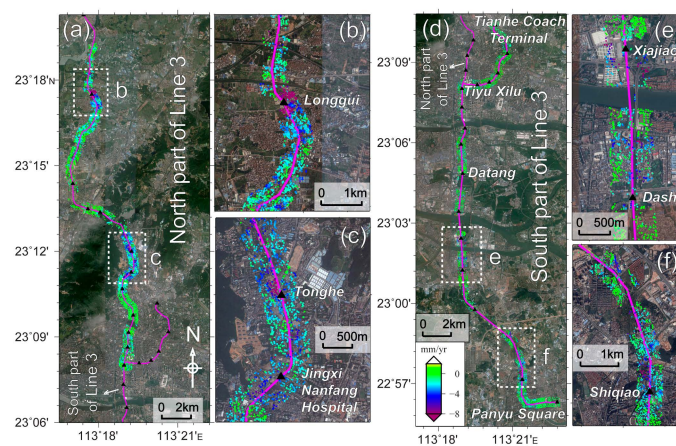


Figure 5. (a) and (d) PALSAR deformation rate maps of Line Three. Regions b, c, e, and f, marked with white dashed rectangles, are four subsiding areas along Line 3, and their enlarged figures are shown in (b), (c), (e), and (f), respectively.

3.3. Subway Network Including Lines One, Four, Five, Six, Eight, and APM

As Figure 6 shows, despite the severe ground subsidence along Line Six, most areas along the metro lines are stable. Lines One, Four, Five, Eight, and APM are stable because they have been in operation more than three years. There are four obvious subsiding areas, outlined by white dashed boxes, along Line Six (Figure 6). As shown in Figure 7a,b, the ground subsidence near the Shabei station (area a in Figure 6) and Tanwei station (area b in Figure 6) are remarkable, with a deformation speed of >8 mm/year. The ground subsidence may be caused by subway construction, because this section was under construction from February 2009 to October 2010. As the field investigation photos show (Figure 7e–g), the subsidence has caused damage to surrounding buildings and threatened local people's lives. Related geological studies reported that these subsiding areas are located above hidden karst [16,38]. Furthermore, we found that junction stations suffers from ground subsidence, such as the Beijing Lu station (Figure 7c) and Yantang station (Figure 7d) because junction stations have more strata loss, especially in unstable geological environments.

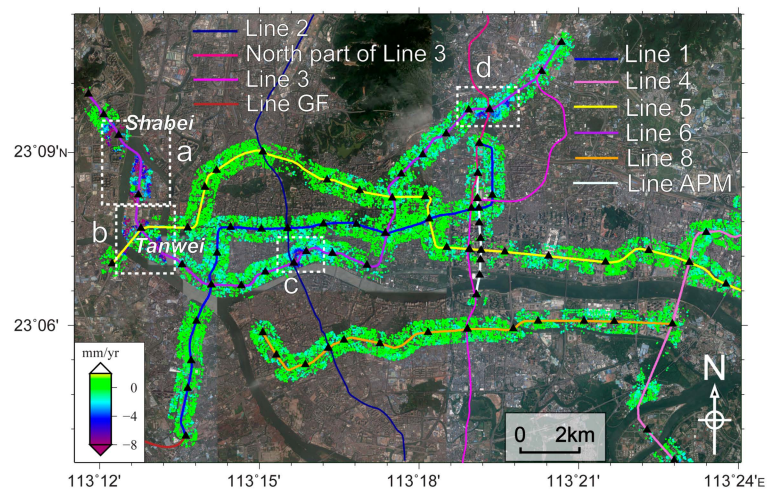


Figure 6. PALSAR deformation rate map of Lines One, Four, Five, Six, Eight, and APM. The dashed rectangles mark the subsiding areas along Line Six, which are detailed in Figure 7a,b.

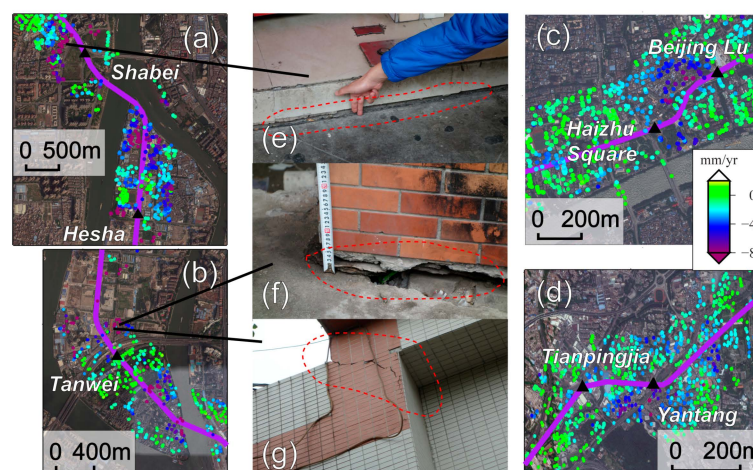


Figure 7. (a–d) The deformation rate maps of four subsiding areas along Line Six. (e–g) The field investigation photos.

3.4. Line GuangFo (Line GF)

Among the Guangzhou metro lines, Line GF suffers the most remarkable subsidence (Figure 8a). The subsidence is concentrated in the section between the Kuiqi Lu and Zumiao stations, with a speed of 6–8 mm/year (Figure 8b), and in the middle section between the Financial Hi-tech Zone and Longxi stations with a speed of >8 mm/year. Subsidence in the latter area is worse, but the settlement trough feature in the former is more noticeable (Figure 8b). The former section is characterized by widely distributed soft soil that is prone to ground subsidence [29]. Therefore, the subsidence there should be caused by tunneling and soft soil consolidation around the tunnel.

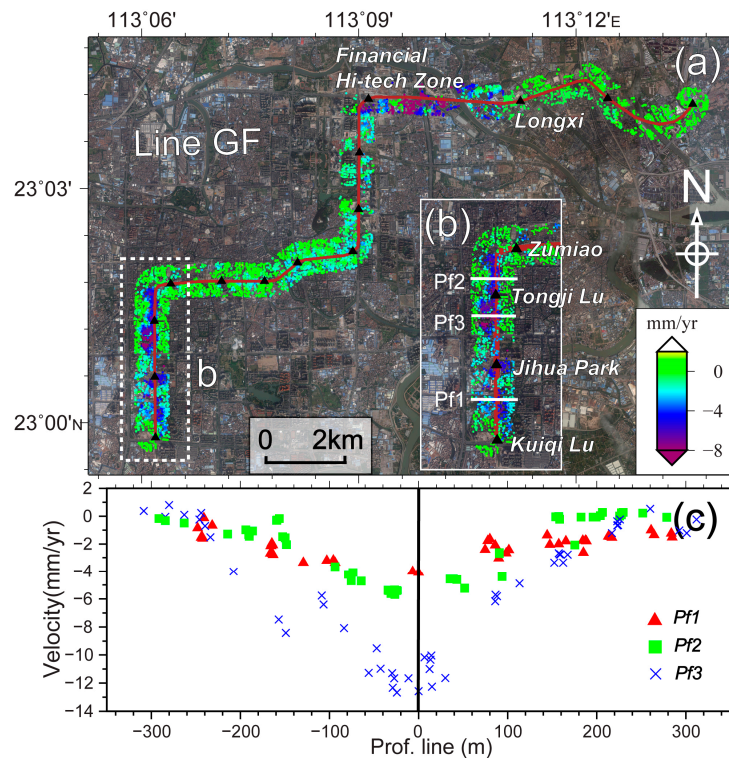


Figure 8. Deformation rate map of Line Guangfo obtained by PALSAR and the subsidence patterns of metro section profiles in soft soil area. (a) The deformation map of Line GF; (b) Metro section from the Kuiqi Lu station to the Zumiao station; (c) Profiles of Pf1, Pf2, and Pf3.

Previous studies found that the long-term subsidence due to subway vehicle loads were responsible for 30–90% of the total tunnel subsidence in soft soil areas [39]. In order to show the ground subsidence patterns of Guangzhou subways in soft soil areas, we selected three settlement profiles: Pf1, Pf2, and Pf3 (Figure 8b), which indicate that the transverse ground settlement approximately follow Gaussian distribution, regardless of the subsidence magnitude (Figure 8c).

4. Tunneling-Induced Ground Subsidence Modeling

Spatio-temporal ground subsidence associated with tunneling is usually modelled with Peck's formula in the spatial domain and with the logistic time model in the temporal domain [23,27]. Using these empirical formulas usually requires a large number of observations. However, because of the limited coverage of traditional geodetic techniques, there are only few geodetic observations available for these empirical formulas. As aforementioned, the IPTA technique, providing wider coverage and denser PT points for subway monitoring, fully meets the requirement of these empirical formulas. Therefore, this study attempted to reveal the long-term spatio-temporal subsidence behavior of subway lines in delta areas with InSAR measurements.

4.1. Peck's Formula and the Logistic Time Model

Peck's formula, shown in Equation (1) [23,24] has been widely used to estimate the spatial distribution of settlement troughs for subway tunnels. The transverse profile of a settlement trough can be approximated by the Gaussian curve [23], as shown in Figure 9a.

$$S(x) = S_{max} \exp\left(-\frac{x^2}{2i^2}\right) \tag{1}$$

where $S(x)$ is the ground subsidence value; x is the horizontal distance to the tunnel centerline in the transverse direction; S_{max} is the maximum subsidence above the tunnel centerline; and i is the settlement trough width, namely the distance from the tunnel centerline to the inflexion point of the curve. S_{max} and i together determine the trough shape. In practice, the two tunnels of the twin-tunnel are excavated in turn. The excavation of first tunnel would inevitably reduce the ground strength around the second one, so tunneling of the second tunnel usually leads to greater ground loss, as shown in Figure 9b [3,40]. So, the ground loss of these two tunnels should be taken account when Peck's formula is applied, as denoted in Equation (2):

$$S_{max} = \frac{\sqrt{\pi}V_L D^2}{2\sqrt{2}i} \tag{2}$$

where V_L is the ground loss ratio per unit length of the tunnel; and D is the diameter of the tunnel. The ground loss is closely related to local hydrogeological conditions and construction. The larger the V_L , the more severe the ground subsidence, and the greater impact to the nearby buildings.

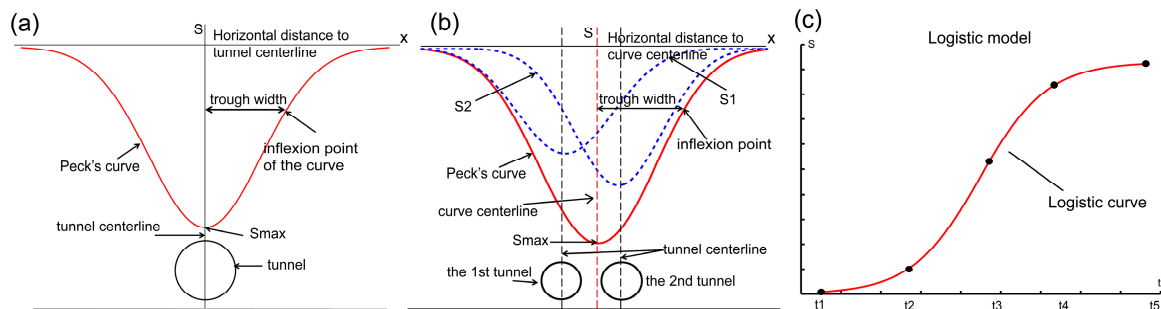


Figure 9. Peck's curve and the logistic time curve. (a) Peck's curve over a single tunnel and (b) Peck's curve over a twin-tunnel. The two dashed lines, S1 and S2, denote the tunneling-induced transverse ground settlement trough, and the red line is considered as the overall effect of S1 and S2; and (c) the logistic time line.

We used the logistic time model to temporally fit the ground subsidence during the subway operation period. This model perfectly reflected the development process of the subway subsidence, including the occurrence, development, and gradually stabilization, as shown in Figure 9c [25]. The logistic time model has been used to analyze the long-term dynamics of tunneling-induced ground subsidence [27] and can be expressed as:

$$W_t = \frac{b}{1 + ae^{-ct}} \tag{3}$$

where W_t is the subsidence value at time (t), parameters a and c are two scale factors of the model, and b denotes the maximum settlement of the function when the settlement is stable.

4.2. Spatial Variation of the Settlement Trough

We chose Line GF to investigate the spatial variation of the settlement trough. We set a 600-m wide buffer along the whole metro line (Figure 8a). The centerline of the buffer coincides with the location of the metro line. Then, to increase the density of PTs, we chose a 20-m buffer area to create a profile along the Line GF. As Equations (1) and (2) show, parameters S_{max} , i , and V_L were used to evaluate the spatial variation and ground loss of the ground settlement trough. Those parameters were estimated using the InSAR measurement. We firstly fit a series of PTs (x_i, y_i) in a transverse ground settlement trough by Peck’s formula, where x_i is the horizontal distance to the tunnel centerline, and y_i is the settlement value corresponding to x_i . The linear regression method was adopted to obtain initial values after taking the log transformation on both sides of Equation (1). Then, a nonlinear least square method [3] was used to estimate the optimal parameters. Eventually, the Root Mean Square Error (RMSE) in Equation (5) and the coefficient of determination (R^2) in Equation (6) were used to evaluate the curve fitting.

$$r = \sum_{i=1}^n (S(x_i) - y_i)^2 \tag{4}$$

$$RMSE = \sqrt{\frac{\sum_{i=1}^n (S(x_i) - y_i)^2}{n}} \tag{5}$$

$$R^2 = \frac{\sum_{i=1}^n (y_i - \sum_{i=1}^n S(x_i)/n)^2}{\sum_{i=1}^n (y_i - \sum_{i=1}^n S(x_i)/n)^2 + \sum_{i=1}^n (S(x_i) - y_i)^2} \tag{6}$$

where n is the number of PTs in the transverse settlement trough. In this study, we selected a profile (Pf2) in Figure 8b to analyze the spatial variation of the transverse settlement trough. The average displacement result fitted by Peck’s formula is shown in Figure 10a. The RMSE and R^2 were 0.63 and 0.93. The result indicates that Peck’s formula is feasible for estimating the transverse settlement trough.

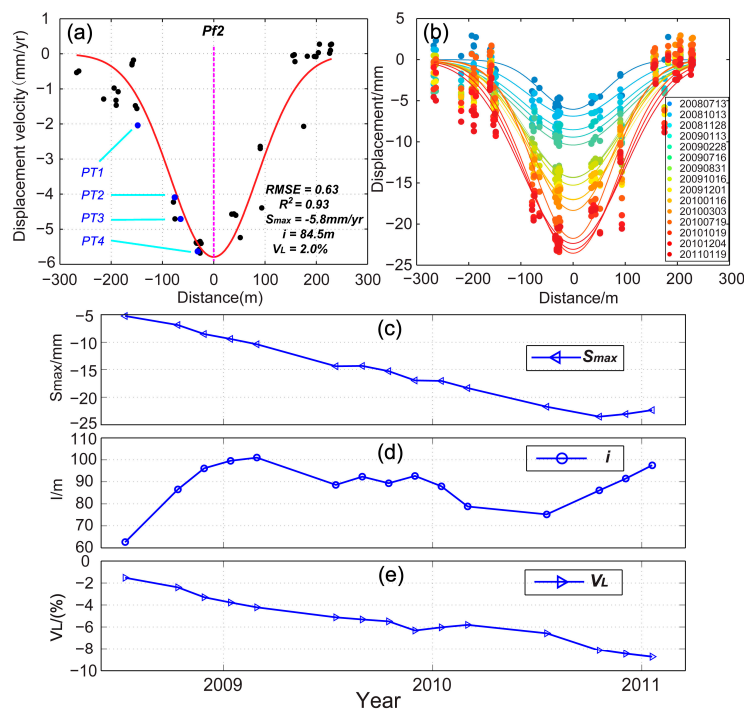


Figure 10. The Pf2 result fitted by Peck’s formula and long-term model parameters of Pf2 based on time-series IPTA. (a) The result fitted by the Peck’s formula; The pink dotted line denotes the curve centerline; (b) time-series settlement trough fitting curves; and (c–e) the variation of structural parameters during the study period.

The profile Pf2 is in the section between the Tongji Lu and Zumiao stations (Figure 8b) and was excavated between December 2007 and July 2008. We analyzed the spatial development of the transverse settlement trough using 15 time-series IPTA results from 13 July 2008 to 19 January 2011. Figure 10b shows that the time-series settlement trough curves perfectly follow Gaussian distribution. In Figure 10c–e, the estimated parameters (S_{max} and V_L) show a linear increasing tendency, indicating that the subsidence is expanding. During this period, the values of S_{max} ranged between -5.2 and -23.6 mm, and V_L ranged between 1.5% and 8.7%. Parameter i did not grow over time but fluctuated between 62.6–101.0 m. To provide an overview of the subsidence behavior along the metro line, we extended the analysis to a wider area from Kuiqi Lu station to Zumiao station, about 4 km, and chose 9 profiles to estimate the structural parameters, according to the PT density. As shown by the results in Table 1, the settlement trough width between Tongji Lu and Zumiao stations was about 65.1–108.2 m, the maximum subsidence value was about -4.6 to -8.0 mm, and the ground loss ratio was 1.6–2.2%.

Table 1. Parameter list of profiles fitted by Peck’s formula.

Metro Segment	R^2	RMSE	$S_{max}/(\text{mm}/\text{year})$	$i/(\text{m})$	$V_L/(\%)$
Kuiqi Lu to Jihua Park	0.73	0.54	-3.9	160.2	2.5%
	0.86	0.79	-5.0	106.7	2.2
Tongji Lu to Zu Miao	0.83	0.76	-4.8	79.8	1.6
	0.95	0.43	-4.6	108.2	2.0
	0.88	1.04	-8.0	65.1	2.1
	0.75	1.08	-6.0	77.0	1.9
	0.77	1.08	-6.2	74.9	1.9
	0.93	0.63	-5.8	84.5	2.0
	0.92	0.62	-5.5	95.1	2.1

4.3. Temporal Variation of PTs

Although the time-series IPTA results and Peck’s formula were used to estimate the spatial development of the Pf2 profile, they could not reflect the ground subsidence dynamics of all PTs on the profile. For this, we adopted the logistic time model to analyze the temporal dynamic variation of PTs. PT1–PT4 are four PTs on the Pf2 profile (Figure 10a). From PT1 to PT4, their horizontal distance to the curve centerline (the pink dotted line in Figure 10a) become smaller. As shown in Figure 11a–d), RMSE and R^2 of the curve fitting are around 0.7 mm and 0.88, respectively, suggesting that the long-term dynamics fitted by the logistic time model are desirable. We found that the subsidence of these four PTs remarkably increased in the first three years and then tended to level off. This is because the dissipation of pore water pressure in the soil layer during the tunneling accelerates in the first three years, which leads to increasing soil consolidation settlement. As the dissipation gradually decreases, the consolidation also slows down. The estimated parameter b in Figure 11 is considered as the maximum settlement of each PT. Note that the maximum settlement is associated with the horizontal distance from the PT to the curve centerline. The smaller the horizontal distance, the greater the absolute value of b .

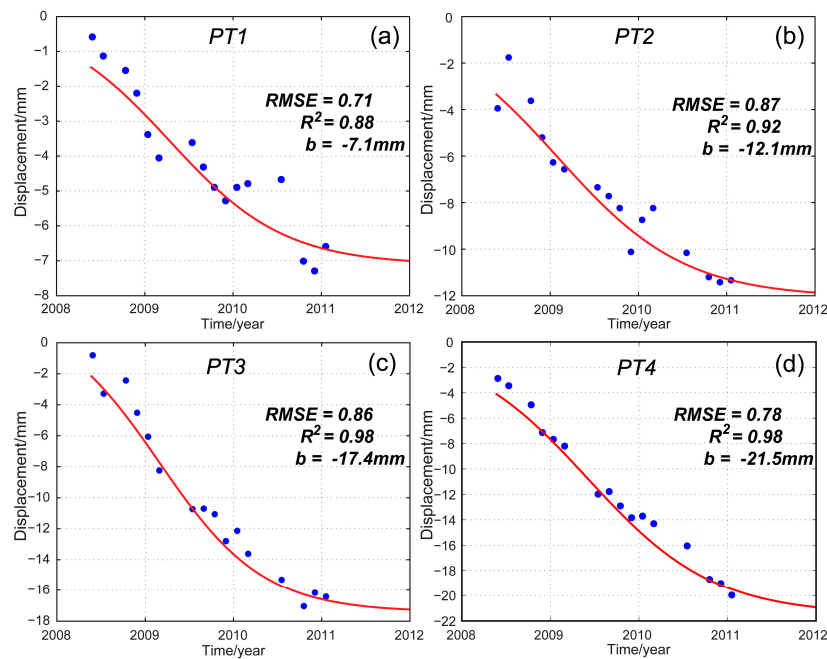


Figure 11. Fitting results of the dynamic variation of four PTs based on the logistic time model: (a) PT1; (b) PT2; (c) PT3; and (d) PT4.

In addition, we estimated the settlement duration of the settlement trough. We considered the ground subsidence was stable, called the ultimate settlement, when the deformation difference of a PT is zero within 100 days. We then estimated the settlement duration t corresponding to the ultimate settlement based on the logistic time model. In fact, different subsiding PTs in the same settlement trough correspond to different cut-off times. The smaller the horizontal distance from the PT to the curve centerline, the longer the duration. So, we only estimated the duration of the PTs around the curve centerline. The maximum duration of PTs on the Pf2 profile was about 2300 days. In other words, without other factors, the ground subsidence would be steady by the end of 2014.

5. Discussion

5.1. Subsidence along Subway Lines in Delta Areas

On the whole, subsidence along subway lines in Guangzhou is limited in scale and scattered in distribution (Figures 4–8). We concluded that the ground subsidence along metro lines is generally distributed close to stations because of the large-scale excavation, that junction stations often suffer severe ground subsidence because of the larger strata loss, and ground subsidence in tunnels mostly occurs in the first three to five years after excavation, and then the tunnels become stable. This was seen in Line One and parts of Lines Two, Three, and Eight. In the soft areas, the ground subsidence was mainly due to the consolidation of clay soil around the tunnel.

Ground subsidence along subways have also been observed in other delta areas, such as Shenzhen [18], Shanghai [17,41], Beijing [19,42,43], and Mexico [44,45]. In different areas, the ground subsidence scales and magnitudes are different. In Shanghai, most metro tunnels are constructed in the soft clay layer with high water content, high compressibility, and low permeability, so non-uniform subsidence (~ 20 mm/year) has often been detected, especially in areas near stations [44]. According to Perissin et al. [17], metro lines that started operating after 2009 have obvious subsidence, while those run since or before 2007 show no significant motion in Shanghai. So, the subsidence of the Shanghai subway network has some similarities with our results for the Guangzhou subway network. In the east of the Pearl River delta, Shenzhen subway's ground subsidence is strongly related to the long-term

land reclamation [18]. However, ground subsidence in the Beijing and Mexico subway networks are dominated by excessive and long-term groundwater extraction, and the subsidence is severe and large-scale (~80 mm/year), rather than scattered small-scale damage [42].

5.2. Ground Subsidence of Subway Network and Geological Conditions

Ground subsidence in delta areas is closely related to local geological conditions [46]. According to the Guangdong Geological Bureau reports [16,47], there are four geological formations (soft soil, loose soil, hidden karst and bedding rock) in the study area (see Figure 12). Most subsidence occurred in the first three geological distributions, especially the soft soil area, because the soil is prone to be compacted under the pressure from engineering constructions (such as tunneling) and clay self-consolidation [46–49]. So there indeed is a spatial correlation between surface subsidence of Guangzhou subway network and geological conditions.

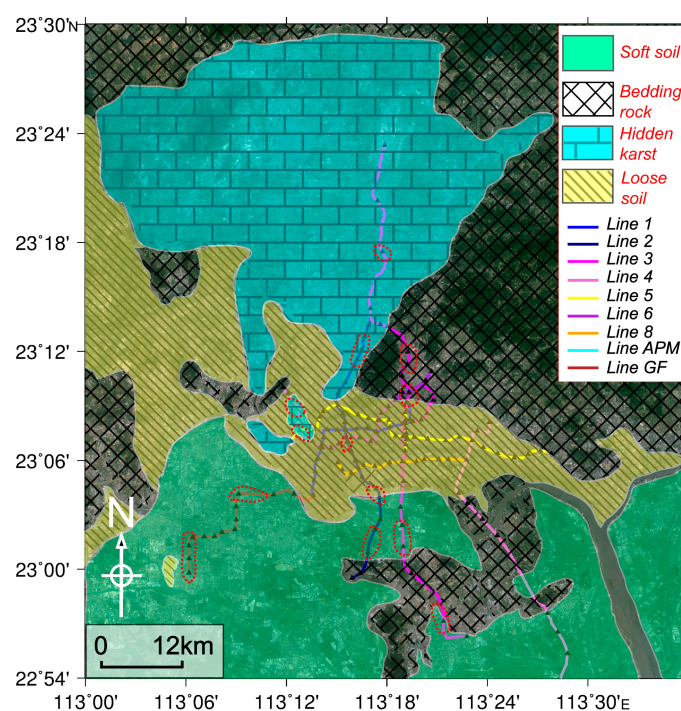


Figure 12. The geological formation, including soft soil, loose soil, hidden karst, and bedding rock, of the Guangzhou subway network. Red dotted circles represent the location of the subsiding areas discussed in Section 3.

The parameters of Peck's Formula are important for analyzing the specific relationship between the settlement trough and geological conditions. Previous studies indicated that the model parameters are related to the soil type [23,24,50,51]. As shown in Table 1, these three parameters have little variation in the section from Tongji Lu to Zumiao stations, which suggests that the geological formations in these areas are similar. We also found that the maximum settlement (S_{max}) and ground loss ratio (V_L) increased with time, while the settlement trough width (i) fluctuated between 62.6 m and 101.0 m (see Figure 10c–e). This result is consistent with previous studies.

5.3. Further Improvement of Subway Monitoring with InSAR

For the evaluation and prediction of the ground subsidence in subway networks, high density and accurate PTs measurements along the subway are important. Although the dense buildings in Guangzhou city provide enough PTs for deformation monitoring, some places above subway lines do not have enough high-quality PTs for parameter inversion due to the limited spatial and temporal

resolution of ENVISAT and ALOS satellites. So, the result can be further improved, if high resolution and short time-span SAR data (TerraSAR-X/TanDEM-X and COSMO-SkyMed) are used. Furthermore, a shorter revisiting cycle of SAR satellite can detect more subsidence evolution details along metro lines, which is helpful for analyzing the mechanisms triggering the geo-hazard, and evaluating potential geo-hazards during subway construction and operation. Therefore, ground subsidence monitoring and evaluation for subway will have to be more systematic.

6. Conclusions

Using the IPTA technique, we accurately mapped the surface deformation of the Guangzhou subway network with ALOS and ASAR images. Both mutual and external data were used to validate the accurate of results, and the comparisons showed the two results are higher than 1 mm/year. We found that, during the study period, Lines One, Four, Five, Eight, and APM were relatively stable, whereas Lines Two, Three, Six, and GF had regional subsidence with the average rate of >8 mm/year. The spatio-temporal analysis showed that the maximum settlement are around [5.2–23.6] mm and its ground loss ratio ranged from 1.5–8.7% between 13 July 2008 and 19 January 2011 in GF line. We also found that the maximum subsidence period can be up to 2300 days in some peak subsidence areas. We believe this study will be a good reference for understanding the ground subsidence behavior of urban subway projects in delta areas.

Acknowledgments: The ENVISAT ASAR data were obtained through the ESA project (No. C1P.14838 and C1P.16734). The ALOS data were provided by the Japan Aerospace Exploration Agency (JAXA) through projects P1229002 and P1390002. This work was supported by National Natural Science Foundation of China (grant numbers 41574005), Shenghua Yuying fund of Central South University and the Project of Autonomous Exploration and Innovation of Central South University (Grant No. 2017zzts172, 2017zzts547 and 2017zzts173).

Author Contributions: Huiqiang Wang, Guangcai Feng and Bing Xu conceive the research work, Huiqiang Wang, Guangcai Feng and Bing Xu wrote the first draft of the paper. Yongping Yu, Zhiwei Li, Yanan Du and Jianjun Zhu contributed to experiment implementation and result interpretation. All authors contributed to paper writing and revision.

Conflicts of Interest: The authors declare no conflict of interest.

Abbreviations

The following abbreviations are used in this manuscript:

ASAR	Advanced Synthetic Aperture Radar
ENVISAT	Environmental Satellite
PALSAR	Phased Array type L-band Synthetic Aperture Radar
ALOS	Advanced Land Observation Satellite
IPTA	Interferometric Point Target Analysis
DEM	Digital Elevation Model
SAR	Synthetic Aperture Radar
LOS	Line-Of-Sight
No.	Number
InSAR	Interferometric Synthetic Aperture Radar
PS-InSAR	Persistent Scatterer Interferometric Synthetic Aperture Radar
PT	Point Target
SRTM	Shuttle Radar Topography Mission
APM	Zhujiang New Town automated people mover system
GF	GuangFo
Pf	Profile+A11B6A12:B17B11:B17

Appendix A

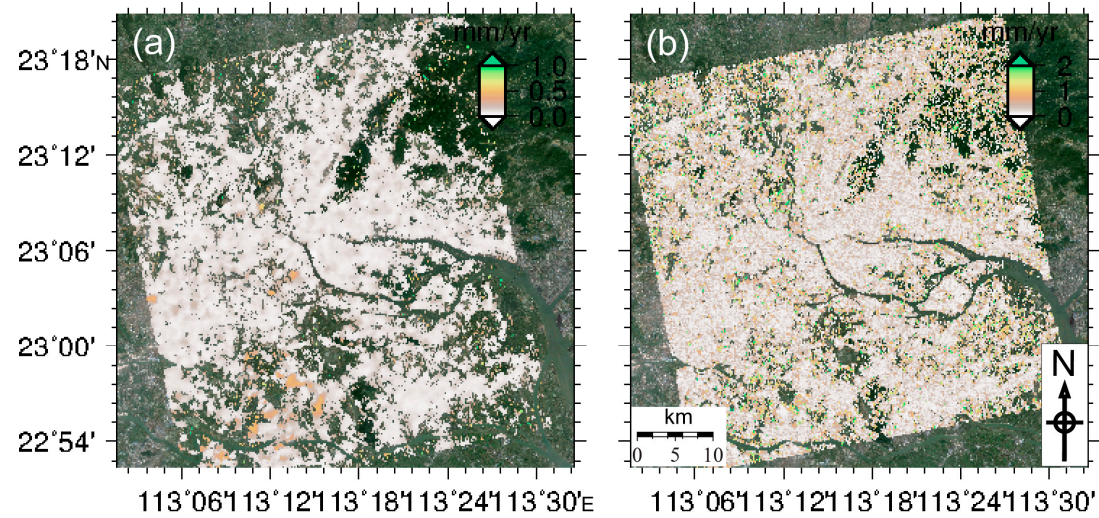


Figure A1. The accuracy of (a) ASAR and (b) PALSAR subsidence rate.

Table A1. Time table of metro line construction in Guangzhou from 1993–2013. Green filling denotes the construction period of metro lines. The triangle symbol is the starting date of construction and the square symbol is the end date of construction. The blue lines cover the monitoring time of SAR images.

Metro	Date													Metro Line Information				
	1993	...	1998	1999	2000	2001	2002	2003	2004	2005	2006	...	2009	2010	...	2013	Num.	Length
Line 1	12.28			06.28													16	18.5
Line 2			07.28											09.25			24	31.8
Line 3						01.26					12.30						29	64.4
Line 4								01.28						09.25			16	46.7
Line 5								05.28						10.15			24	31.9
Line 6									06.28							12.28	22	24.5
Line 8					08.23									09.25			13	18.5
Line GF							10.11							11.03			14	32.2
Line APM										06.30				11.08			9	3.94

Table A2. ASAR/PALSAR data information. Perp_B (m) denotes the Perpendicular Baseline (m) and Temp_B (day) represents the Temporal Baseline (day).

No.	SAR Sensor	Acquisition Date	Perp_B (m)	Temp_B (day)	SAR Sensor	Acquisition Date	Perp_B (m)	Temp_B (day)
1	ASAR	2007/04/23	-63.941	-525	PALSAR	2007/07/11	-109.624	-920
2	ASAR	2007/05/28	-20.586	-490	PALSAR	2007/08/26	117.551	-874
3	ASAR	2007/07/02	201.324	-455	PALSAR	2007/10/11	320.738	-828
4	ASAR	2007/08/06	359.937	-420	PALSAR	2008/01/11	642.339	-736
5	ASAR	2007/09/10	428.338	-385	PALSAR	2008/05/28	1044.648	-598
6	ASAR	2007/10/15	223.502	-350	PALSAR	2008/07/13	-893.790	-552
7	ASAR	2007/11/19	272.394	-315	PALSAR	2008/10/13	-1747.478	-460
8	ASAR	2008/05/12	82.061	-140	PALSAR	2008/11/28	-1547.674	-414
9	ASAR	2008/06/16	-16.821	-105	PALSAR	2009/01/13	-1247.589	-368
10	ASAR	2008/07/21	52.467	-70	PALSAR	2009/02/28	-1251.581	-322
11	ASAR	2008/08/25	464.493	-35	PALSAR	2009/07/16	-595.590	-184
12	ASAR	2008/09/29	0	0	PALSAR	2009/08/31	-305.935	-138
13	ASAR	2008/11/03	427.851	35	PALSAR	2009/10/16	-178.100	-92
14	ASAR	2008/12/08	-86.414	70	PALSAR	2009/12/01	-243.643	-46
15	ASAR	2009/01/12	249.802	105	PALSAR	2010/01/16	0	0
16	ASAR	2009/04/27	-115.195	210	PALSAR	2010/03/03	341.146	46
17	ASAR	2009/06/01	-96.704	245	PALSAR	2010/07/19	595.503	184
18	ASAR	2009/08/10	322.399	315	PALSAR	2010/10/19	871.944	276
19	ASAR	2009/09/14	263.386	350	PALSAR	2010/12/04	836.577	322
20	ASAR	2009/10/19	188.442	385	PALSAR	2011/01/19	1156.677	368
21	ASAR	2009/11/23	203.992	420				
22	ASAR	2009/12/28	-85.578	455				
23	ASAR	2010/02/01	210.405	490				
24	ASAR	2010/03/08	234.188	525				
25	ASAR	2010/04/12	393.560	560				
26	ASAR	2010/05/17	18.411	595				
27	ASAR	2010/06/21	279.802	630				
28	ASAR	2010/07/26	87.535	665				
29	ASAR	2010/0810	374.686	700				

Appendix B

We simulated a subsidence bowl, given that the magnitude of the east–west and north–south components are about 1/5 the vertical component in a LOS deformation. The detailed three-dimensional displacement components are shown in Figure A2a–c. We used the unit vector of ascending ENVISAT ASAR geometry $[-0.379, 0.080, 0.922]$ to simulate the LOS displacement in Figure A2d. We then calculated the vertical deformation with non-horizontal assumption ($\text{los}/0.922$) in Figure A2e. Then we obtained the difference between the real and the estimated vertical component with the assumption in Figure A2f. We found that the maximum difference is about 0.05, significantly smaller than the vertical component. Therefore, the non-horizontal assumption for calculating vertical deformation in this case is generally reasonable because the magnitude of residue is around the level of uncertainty of InSAR measurement.

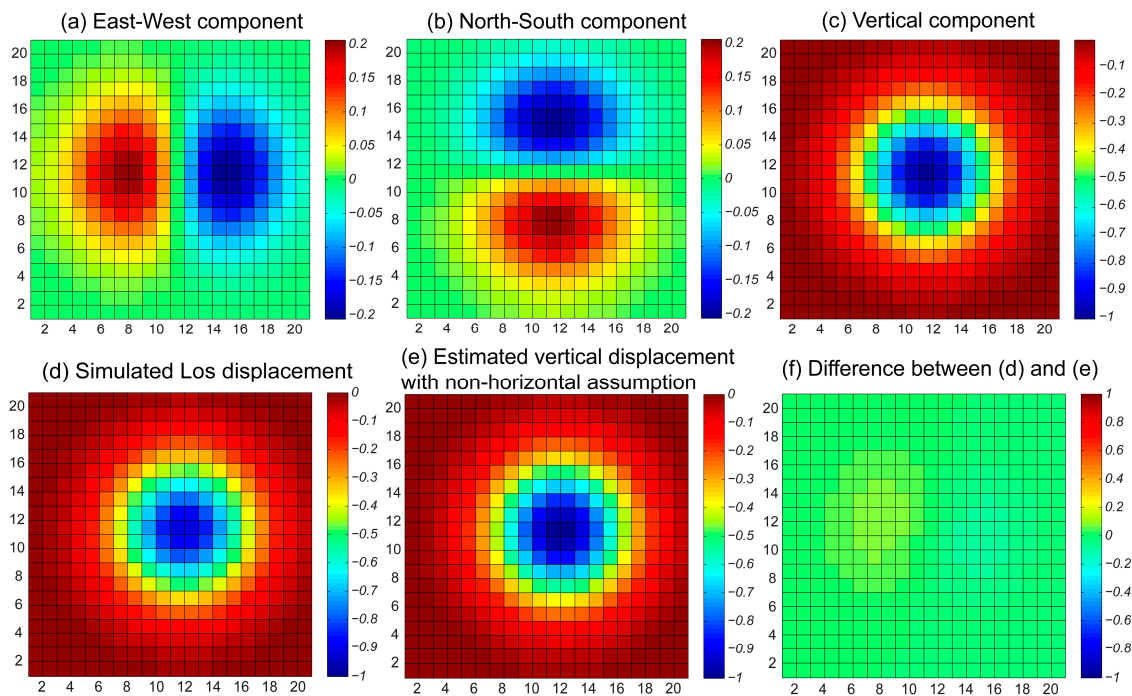


Figure A2. Simulated three-dimensional (3D) displacement components in (a) the east–west directions; (b) north–south directions; and (c) vertical directions; (d) Simulated LOS displacement; (e) estimated vertical displacement with non-horizontal assumption; (f) the vertical residue estimated by difference between (d) simulated LOS displacement and (e) with non-horizontal assumption.

References

1. Kontogianni, V.A.; Stiros, S.C. Induced deformation during tunnel excavation: Evidence from geodetic monitoring. *Eng. Geol.* **2005**, *79*, 115–126. [[CrossRef](#)]
2. Kavvadas, M.J. Monitoring ground deformation in tunneling: Current practice in transportation tunnels. *Eng. Geol.* **2005**, *79*, 93–113. [[CrossRef](#)]
3. Ma, L.; Ding, L.; Luo, H. Non-linear description of ground settlement over twin tunnels in soil. *Tunn. Undergr. Space Technol.* **2014**, *42*, 144–151. [[CrossRef](#)]
4. Wu, J.C.; Hu, F.M. Monitoring ground subsidence along the Shanghai maglev zone using TerraSAR-X images. *IEEE Geosci. Remote Sens. Lett.* **2017**, *14*, 117–121. [[CrossRef](#)]
5. Massonnet, D.; Rossi, M.; Carmona, C.; Adragna, F.; Peltzer, G.; Feigl, K. The displacement field of the Landers earthquake mapped by radar interferometry. *Nature* **1993**, *364*, 138–142. [[CrossRef](#)]
6. Ferretti, A.; Prati, C.; Rocca, F.L. Permanent Scatterers in SAR Interferometry. *IEEE Trans. Geosci. Remote Sens.* **2001**, *39*, 8–20. [[CrossRef](#)]
7. Berardino, P.; Fornaro, G.; Lanari, R.; Sansosti, E. A new algorithm for surface deformation monitoring based on small baseline differential SAR Interferograms. *IEEE Trans. Geosci. Remote Sens.* **2002**, *40*, 2375–2383. [[CrossRef](#)]
8. Ding, C.; Feng, G.; Li, Z.; Shan, X.; Du, Y.; Wang, H. Spatio-temporal error sources analysis and accuracy improvement in Landsat 8 image ground displacement measurements. *Remote Sens.* **2016**, *8*, 937. [[CrossRef](#)]
9. Feng, G.; Li, Z.; Xu, B.; Shan, X.; Zhang, L.; Zhu, J. Coseismic deformation of the 2015 Mw 6.4 Pishan, China, earthquake estimated from Sentinel-1a and ALOS2 data. *Seismol. Res. Lett.* **2016**, *87*, 800–806. [[CrossRef](#)]
10. Hu, J.; Ding, X.L.; Zhang, L.; Sun, Q.; Li, Z.W.; Zhu, J.J.; Lu, Z. Estimation of 3-D surface displacement based on InSAR and deformation modeling. *IEEE Trans. Geosci. Remote Sens.* **2017**, *55*, 2007–2016. [[CrossRef](#)]
11. Hu, J.; Li, Z.W.; Ding, X.L.; Zhu, J.J.; Zhang, L.; Sun, Q. Resolving three-dimensional surface displacements from InSAR measurements: A review. *Earth-Sci. Rev.* **2014**, *133*, 1–17. [[CrossRef](#)]
12. Fu, H.; Zhu, J.; Wang, C.; Wang, H.; Zhao, R. Underlying topography estimation over forest areas using high-resolution P-band single-baseline PolInSAR data. *Remote Sens.* **2017**, *9*, 363. [[CrossRef](#)]

13. Zhao, R.; Li, Z.W.; Feng, G.C.; Wang, Q.J.; Hu, J. Monitoring surface deformation over permafrost with an improved SBAS-InSAR algorithm: With emphasis on climatic factors modeling. *Remote Sens. Environ.* **2016**, *184*, 276–287. [[CrossRef](#)]
14. Du, Y.N.; Zhang, L.; Feng, G.C.; Lu, Z.; Sun, Q. On the accuracy of topographic residuals retrieved by MTInSAR. *IEEE Trans. Geosci. Remote Sens.* **2017**, *99*, 1–13. [[CrossRef](#)]
15. Yang, Z.F.; Li, Z.W.; Zhu, J.J.; Preusse, A.; Yi, H.W.; Wang, Y.J.; Papst, M. An extension of the insar-based probability integral method and its application for predicting 3-D mining-induced displacements under different extraction conditions. *IEEE Trans. Geosci. Remote Sens.* **2017**, *99*, 1–11. [[CrossRef](#)]
16. Zhao, Q.; Lin, H.; Jiang, L.M.; Chen, F.L.; Cheng, S.L. A study of ground deformation in the Guangzhou urban area with Persistent Scatterer Interferometry. *Sensors* **2009**, *9*, 503–518. [[CrossRef](#)] [[PubMed](#)]
17. Perissin, D.; Wang, Z.; Lin, H. Shanghai subway tunnels and highways monitoring through Cosmo-Skymed Persistent Scatterers. *ISPRS-J. Photogramm. Remote Sens.* **2012**, *73*, 58–67.
18. Xu, B.; Feng, G.C.; Li, Z.W.; Wang, Q.J.; Wang, C.C.; Xie, R.A. Coastal subsidence monitoring associated with land reclamation using the Point Target Based SBAS-InSAR method: A case study of Shenzhen, China. *Remote Sens.* **2016**, *8*, 652. [[CrossRef](#)]
19. Chen, W.F.; Gong, H.L.; Chen, B.B.; Liu, K.S.; Gao, M.; Zhou, C.F. Spatiotemporal evolution of land subsidence around a subway using insar time-series and the entropy method. *GISci. Remote Sens.* **2016**, *54*, 78–94. [[CrossRef](#)]
20. Falorni, G.; Iannacone, J.P. Signature of Tunneling-Induced Ground Deformation in Urban Areas Revealed by Time Series Analysis. In Proceedings of the Vancouver TAC, Vancouver, BC, Canada, 26–28 October 2014.
21. García Robles, J.; Salvá Gomar, B.; Arnaud, A. Non-Linear Motion Detection using SAR Images in Urban Tunnelling. In Proceedings of the ITA World Tunnel Congress, Dubrovnik, Croatia, 22–28 May 2015.
22. Barla, G.; Tamburini, A.; Del Conte, S.; Giannico, C. Insar monitoring of tunnel induced ground movements. *Geomech. Tunn.* **2016**, *9*, 15–22. [[CrossRef](#)]
23. Peck, R.B. Deep excavations and tunneling in soft ground. In Proceedings of the 7th International Conference on Soil Mechanics and Foundation Engineering, Mexico City, Mexico, 22–23 October 1969; pp. 225–290.
24. O'Reilly, M.P.; New, B.M. Settlements above tunnels in the United Kingdom—Their magnitude and prediction. In Proceedings of the Tunnelling, Institute of Mining Metallurgy, London, UK, 7–11 June 1982; pp. 173–181.
25. Xu, H.Z.; Shi, B.; Li, X.H. Logistic growth model and its applicability for predicting settlement during the whole process. *Rock Soil Mech.* **2005**, *26*, 387–391.
26. Zhang, W.Z.; Zou, Y.F.; Ren, X.F. Research on logistic model in forecasting subsidence single-point during mining. *J. Min. Saf. Eng.* **2009**, *26*, 486–489.
27. Mo, Y.; Yue, H.; Hu, B.; Wu, B. A study of logistic equation applied to predicting ground settlement induced by subway tunneling work. *Chin. J. Eng. Geophys.* **2010**, *7*, 115–119.
28. Yang, Z.F.; Li, Z.W.; Zhu, J.J.; Yi, H.W.; Hu, J.; Feng, G.C. Deriving Dynamic Subsidence of Coal Mining Areas Using InSAR and Logistic Model. *Remote Sens.* **2017**, *9*, 125. [[CrossRef](#)]
29. Chen, F.; Lin, H.; Zhang, Y.; Lu, Z. Ground subsidence geo-hazards induced by rapid urbanization: Implications from InSAR observation and geological analysis. *Nat. Hazards Earth Syst. Sci.* **2012**, *12*, 935–942. [[CrossRef](#)]
30. Ao, M.S.; Wang, C.C.; Xie, R.; Zhang, X.; Hu, J.; Du, Y.N.; Li, Z.; Zhu, J.; Dai, W.; Kuang, C. Monitoring the land subsidence with Persistent Scatterer Interferometry in Nansha district, Guangdong, China. *Nat. Hazards* **2015**, *75*, 2947–2964. [[CrossRef](#)]
31. Liao, H.Y. *Technology for Shield Tunnel in Mixed Face Ground Conditions: Study & Practice in Shield Tunneling Projects of Guangzhou Metro*; China Architecture & Building Press: Beijing, China, 2012. (In Chinese)
32. Werner, C.; Wegmüller, U.; Strozzi, T.; Wiesmann, A. Interferometric Point Target Analysis for deformation mapping. In Proceedings of the 2003 IEEE International Geoscience and Remote Sensing Symposium, Amherst, MA, USA, 21–25 July 2003.
33. Stramondo, S.; Bozzano, F.; Marra, F.; Wegmüller, U.; Cinti, F.R.; Moro, M.; Saroli, M. Subsidence induced by urbanisation in the city of Rome detected by advanced InSAR technique and geotechnical investigations. *Remote Sens. Environ.* **2008**, *112*, 3160–3172. [[CrossRef](#)]
34. Jiang, H.; Feng, G.; Wang, T.; Bürgmann, R. Toward full exploitation of coherent and incoherent information in Sentinel—1 tops data for retrieving surface displacement: Application to the 2016 Kumamoto (Japan) earthquake. *Geophys. Res. Lett.* **2017**, *44*, 1758–1767. [[CrossRef](#)]

35. Wang, L.; Gao, H.; Feng, G. InSAR and GPS inversion for source parameters of the 2016 mw6.4 Meinong, Taiwan earthquake. *Chin. J. Geophys.* **2017**, *60*, 2578–2588.
36. Feng, G.; Jónsson, S.; Klinger, Y. Which fault segments ruptured in the 2008 Wenchuan earthquake and which did not? new evidence from near—Fault 3d surface displacements derived from SAR image offsets. *Bull. Seismol. Soc. Am.* **2017**, *107*, 1–16. [[CrossRef](#)]
37. Zhang, G.; Shan, X.; Zhang, Y.; Hetland, E.; Qu, C.; Feng, G. Blind thrust rupture of the 2015 m w, 6.4 pishan earthquake in the northwest Tibetan plateau by joint inversion of insar and seismic data. *J. Asian Earth Sci.* **2016**, *132*, 118–128. [[CrossRef](#)]
38. Huang, J.M.; Guo, Y.; Hu, R.Q.; Zhou, Z.Y. Analysis of land subsidence in Jinshazhou area, Guangzhou city. *Chin. J. Geol. Hazard Cont.* **2013**, *24*, 61–67. (In Chinese)
39. Shirlaw, J.N. Observed and calculated pore pressures and deformations induced by an earth balance shield: Discussion. *Can. Geotech. J.* **2011**, *32*, 181–189. [[CrossRef](#)]
40. Suwansawat, S.; Einstein, H.H. Describing settlement troughs over twin tunnels using a superposition technique. *J. Geotech. Geoenviron. Eng.* **2007**, *133*, 445–468. [[CrossRef](#)]
41. Shen, S.L.; Wu, H.N.; Cui, Y.J.; Yin, Z.Y. Long-term settlement behaviour of metro tunnels in the soft deposits of Shanghai. *Tunn. Undergr. Space Technol.* **2014**, *40*, 309–323. [[CrossRef](#)]
42. Ge, D.Q.; Zhang, L.; Li, M.; Liu, B.; Wang, Y. Beijing subway tunnelings and high-speed railway subsidence monitoring with PSInSAR and TerraSAR-X data. In Proceedings of the 2016 IEEE International Geoscience and Remote Sensing Symposium, Beijing, China, 10–15 July 2016.
43. Duan, G.Y.; Gong, H.L.; Liu, H.; Zhang, Y.; Chen, B.B.; Lei, K.C. Monitoring and analysis of land subsidence along Beijing-Tianjin inter-city railway. *J. Indian Soc. Remote Sens.* **2016**, *44*, 1–17.
44. Batuhan, O.; Timothy, H.D.; Shimon, W.; Enrique, C.C.; Jiang, Y. Mexico City subsidence observed with Persistent Scatterer InSAR. *Int. J. Appl. Earth Obs. Geoinf.* **2011**, *13*, 1–12.
45. Yan, Y.J.; Doin, M.P.; Lopez-Quiroz, P.; Tupin, F.; Fruneau, B.; Pinel, V. Mexico City subsidence measured by InSAR time series: Joint analysis using PS and SBAS approaches. *IEEE J. Sel. Top. Appl. Earth Obs. Remote Sens.* **2012**, *5*, 1312–1326. [[CrossRef](#)]
46. Du, Y.N.; Feng, G.C.; Peng, X.; Li, Z.W. Subsidence Evolution of the Leizhou Peninsula, China, Based on InSAR Observation from 1992 to 2010. *Appl. Sci.* **2017**, *7*, 466. [[CrossRef](#)]
47. Ren, D.J.; Shen, S.L.; Cheng, W.C.; Zhang, N.; Wang, Z.F. Geological formation and geo-hazards during subway construction in Guangzhou. *Environ. Earth Sci.* **2016**, *75*, 1–14. [[CrossRef](#)]
48. Liu, J.F.; Qi, T.Y.; Wu, Z.R. Analysis of ground movement due to metro station driven with enlarging shield tunnels under building and its parameter sensitivity analysis. *Tunn. Undergr. Space Technol.* **2012**, *28*, 287–296. [[CrossRef](#)]
49. Cui, Z.D.; Tan, J. Analysis of long-term settlements of Shanghai subway line 1 based on the in situ monitoring data. *Nat. Hazards.* **2015**, *75*, 465–472. [[CrossRef](#)]
50. Attewell, P.B.; Farmer, I.W. Ground deformations resulting from shield tunneling in London clay. *Can. Geotech. J.* **1974**, *11*, 380–395. [[CrossRef](#)]
51. Lei, M.; Wang, Q.; Liu, X.; Xu, B.; Zhang, H. Influence of ocean tidal loading on InSAR offshore areas deformation monitoring. *Geod. Geodyn.* **2017**, *8*, 70–76. [[CrossRef](#)]

